The Extreme CNO-enhanced Composition of the Primitive Iron-poor Dwarf Star J0815+4729[*]

Jonay I. González Hernández[1,2] , David S. Aguado[3] , Carlos Allende Prieto[1,2] , Adam J. Burgasser[4] , and Rafael Rebolo[1,2,5]

[1] Instituto de Astrofísica de Canarias, Vía Láctea, E-38205 La Laguna, Tenerife, Spain; jonay@iac.es
[2] Universidad de La Laguna, Departamento de Astrofísica, E-38206 La Laguna, Tenerife, Spain
[3] Institute of Astronomy, University of Cambridge, Madingley Road, Cambridge CB3 0HA, UK
[4] Center for Astrophysics and Space Science, University of California San Diego, La Jolla, CA 92093, USA
[5] Consejo Superior de Investigaciones Científicas, E-28006 Madrid, Spain

Abstract

We present an analysis of high-resolution Keck/HIRES spectroscopic observations of J0815+4729, an extremely carbon-enhanced, iron-poor dwarf star. These high-quality data allow us to derive a metallicity of [Fe/H] = -5.49 ± 0.14 from the three strongest Fe I lines and to measure a high [Ca/Fe] = 0.75 ± 0.14. The large carbon abundance of A(C) = 7.43 ± 0.17 (or [C/Fe] $\sim 4.49 \pm 0.11$) places this star in the upper boundary of the low-carbon band in the A(C)–[Fe/H] diagram, suggesting no contamination from a binary AGB companion. We detect the oxygen triplet at 777 nm for the first time in an ultra-metal-poor star, indicating a large oxygen-to-iron abundance ratio of [O/Fe] = 4.03 ± 0.12 (A(O) = 7.23 ± 0.14), significantly higher than the previously most metal-poor dwarf J2209–0028 with an oxygen triplet detection with [O/Fe] ~ 2.2 dex at [Fe/H] ~ -3.9. Nitrogen is also dramatically enhanced with (A(N) = 6.75 ± 0.08) and an abundance ratio [N/Fe] $\sim 4.41 \pm 0.08$. We also detect Ca, Na, and Mg, while providing upper limits for eight other elements. The abundance pattern of J0815+4729 resembles that of HE 1327–2326, indicating that both are second-generation stars contaminated by a $\sim$21–27 $M_\odot$ single, zero-metallicity, low-energy supernova with very little mixing and substantial fallback. The absence of lithium implies an upper limit abundance A(Li) < 1.3 dex, about 0.7 dex below the detected Li abundance in J0023+0307, which has a similar metallicity, exacerbating the cosmological lithium problem.

Unified Astronomy Thesaurus concepts: Early universe (435); Halo stars (699); Chemical abundances (224); Overabundances (1192); Stellar abundances (1577); Big Bang nucleosynthesis (151); Explosive nucleosynthesis (503); Population III stars (1285); Core-collapse supernovae (304)

1. Introduction

Some of the most metal-poor low-mass stars formed in the very early universe are still observable in the Galactic halo. These stars are expected to originate from a mixture of primordial material from the Big Bang and matter ejected from the few first supernovae (SNe). The chemical pattern of these stars holds crucial information about the early epochs of the universe, such as the properties of the first stars (so-called Population III stars) and first SNe, the early chemical evolution of the universe, and the formation of low-mass stars in the early universe.

Over the past few decades, a significant observational effort has been focused on the detection and characterization of the most metal-poor stars. These are initially identified in large spectroscopic surveys such as Hamburg/ESO (HE; Christlieb et al. 2001) or Sloan Digital Sky Survey (SDSS; York et al. 2000), or in narrow-filter photometric surveys such as Skymapper (Keller et al. 2007) or Pristine (Starkenburg et al. 2017). Follow-up high-quality medium- and high-resolution spectra are used to confirm the metal-poor nature of these stars and provide their detailed chemical abundances. To date, only seven stars are known to have [Fe/H] < −5 (Christlieb et al. 2004; Frebel et al. 2008; Keller et al. 2014; Bonifacio et al. 2015; Aguado et al. 2018b, 2018a; Nordlander et al. 2019) and

all are carbon-enhanced (CEMP) with carbon abundances in the range A(C) = 6–7.5 dex.

The metal-poor halo star SDSS J081554.26+472947.5 was first identified in the SDSS/BOSS spectroscopic database and confirmed as an extremely carbon-rich, iron-poor star by Aguado et al. (2018b) using follow-up medium-resolution observations obtained with OSIRIS at the 10.4 m GTC telescope. Here we present new high-resolution high-quality High Resolution Echelle Spectrometer (HIRES) spectroscopic observations revealing the unique abundance pattern of this star.

2. Observations

High-resolution spectroscopic observations of J0815+4729 were carried out on 2018 December 10 (UT) using the HIRES (Vogt et al. 1994) on the Keck I telescope at the Maunakea observatory. We used the cross-disperser HIRESr with a slit width of 1″15 and 2 × 2 binning, providing spectra over the range $\lambda\lambda$340–780 nm at a resolving power of $R \sim 37,500$. Seven spectra of 2400 s were obtained over a seeing of 1″0–1″3 and airmasses of 1.1–1.3. The individual spectra had signal-to-noise ratios (S/Ns) of 15, 21, 31, 40, 42 at λ = 395, 440, 518, 670, and 775 nm, respectively. We used the MAKEE software to reduce the data, and the IRAF package ECHELLE to calibrate the individual spectra and normalize each order using a third-order polynomial continuum correction.

Radial velocities (RVs) were derived by cross-correlating each barycenter-corrected observed spectrum with a synthetic

---

[*] Based on observations made with Keck I telescope at Maunakea Observatory, Hawaii, USA.
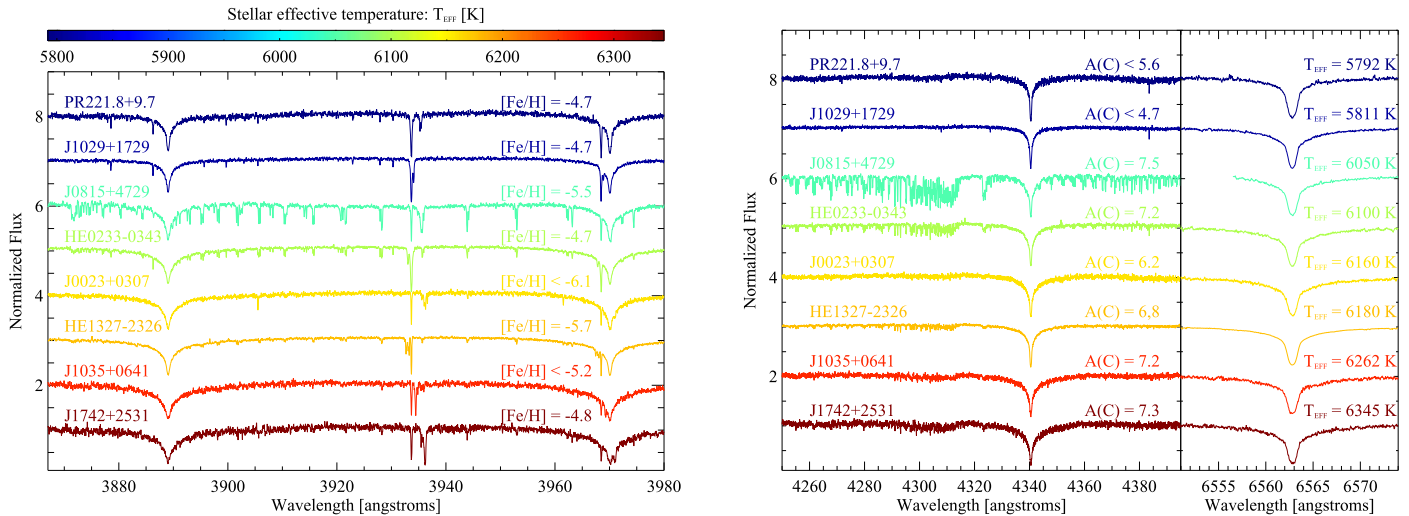
Figure 1. Keck/HIRES high-resolution spectra of the star J0815+4729 in three different spectral regions, compared to VLT/UVES high-resolution spectra of other unevolved, extremely iron-poor stars (Frebel et al. 2008; Caffau et al. 2012; Hansen et al. 2014; Bonifacio et al. 2018; Starkenburg et al. 2018; Aguado et al. 2019). The stars are sorted and colored by their effective temperature from top to bottom.

spectrum in the range $\lambda\lambda 418$–432 nm. This region encompasses many individual lines of the CH A–X band that are pronounced in this carbon-enriched star (see Figure 1). We measure a mean radial velocity of $v_R = -123.1 \pm 0.4$ km s^{-1}, consistent with the $v_R = -95 \pm 23$ km s^{-1} reported in the discovery paper from the GTC/OSIRIS spectrum (Aguado et al. 2018b), with $v_R = -118 \pm 5$ km s^{-1} determined from the discovery SDSS/BOSS spectrum (Dawson et al. 2013) and with $v_R \sim -124.4$ km s^{-1} from a LAMOST spectrum (Li et al. 2018). We find no evidence of RV variability from these measurements.

The HIRES spectra were RV corrected, coadded, and rebinned using wavelength steps of 0.030, 0.042, and 0.055 Å pixel^{-1} in the blue ($\lambda\lambda 340$–473 nm), green ($\lambda\lambda 478$–631 nm), and red ($\lambda\lambda 632$–782 nm) detector regions, respectively. In Figure 1 we compare the HIRES spectrum of J0815+4729 to Very Large Telescope (VLT)/UVES spectra of other extremely iron-poor stars available in the ESO[6] Archive Science Portal.[7] For proper comparison, we have processed the UVES data similarly: individual spectra have been normalized using a fifth-order polynomial continuum correction based on our own automated IDL-based routine, corrected for barycentric motion and star's radial velocity, and coadded and rebinned to the same wavelength step as the final HIRES spectrum.

3. Stellar Parameters

Following Aguado et al. (2019) we analyzed the spectrum of J0815+4729 using a grid of synthetic spectral models spanning $-7 \leqslant$ [Fe/H] $\leqslant -4$, $-1 \leqslant$ [C/Fe] $\leqslant 7$, 4750 K $\leqslant T_{\rm eff} \leqslant$ 7000 K, and $1 \leqslant \log(g) \leqslant 5$, computed with the code ASSϵT (Koesterke et al. 2008) and model atmospheres from Kurucz ATLAS9 (Mészáros et al. 2012). The microturbulence, ξ, and α-element abundance were fixed at 2 km s^{-1} and [α/Fe] = 0.4, respectively. We used the FERRE code[8] (see, e.g., Aguado et al.

2017) to fit the whole HIRES spectrum of J0815+4729 and separately to fit only the Balmer H I lines. Both methods provide the same effective temperature, $T_{\rm eff} \sim 6050$ K, and surface gravity, $\log g = 4.7$ dex. This $T_{\rm eff}$ is lower than our previous estimates from medium-resolution OSIRIS, BOSS, and ISIS spectra, the former yielding $T_{\rm eff} = 6215 \pm 82$ K (Aguado et al. 2018b). We also estimate a $T_{\rm IRFM} \sim 6196 \pm 185$ K by applying the infrared flux method (González Hernández & Bonifacio 2009) to Two Micron All-Sky Survey (2MASS) J and Johnson V magnitudes (the latter transformed from SDSS g and r photometry), and assuming a reddening of $E(B–V) = 0.073$ (Schlegel et al. 1998). Note that 2MASS HK_s magnitudes were not used due to their large uncertainties. We also apply the $T_{\rm eff}$–$(V–J)$, [Fe/H] calibration in Casagrande et al. (2010) to estimate a $T_{\rm IRFM} \sim 6237 \pm 228$ K, consistent with the previous values.

A recent estimate of the stellar parameters that relies on *Gaia* DR2 data provides $T_{\rm eff} = 6034 \pm 56$ K and $\log g = 4.6 \pm 0.1$ dex (Sestito et al. 2019), consistent with our HIRES analysis. From the accurate *Gaia* parallax ($\omega = 0.444 \pm 0.084$ mas), these authors derived a distance of $D = 1.59 \pm 0.07$ kpc and inferred an inner-halo Galactic orbit (see supplementary online material in Sestito et al. 2019) similar to other iron-poor dwarf stars such as J0023+0307. While the highly eccentric orbit of J0023+0307 ($\epsilon = 0.88 \pm 0.04$) remains relatively close to the Galactic plane ($|Z| < 2.3$ kpc), the less eccentric orbit of J0815+4729 ($\epsilon = 0.32 \pm 0.04$) is roughly spherical with a radius of about 10 kpc. We adopt $T_{\rm eff} = 6050 \pm 100$ K and $\log g = 4.6 \pm 0.2$ dex for our chemical abundance modeling.

4. Chemical Analysis

Chemical abundance analysis has been carried out in 1D local thermodynamic equilibrium (LTE) using the SYNPLE[9] code and an ATLAS9 model atmosphere $T_{\rm eff}/\log g/$[Fe/H] = 6050/4.6/-5. We adopt a microturbulence of $\xi = 1.5$ km s^{-1} suitable for metal-poor dwarf stars (Barklem et al. 2005). We performed a fit to different spectral features of the HIRES

Table 1
Element 1D-LTE Abundances of J0815+4729

Species	$A_\odot(X)$	$A(X)$	$\delta A(X)$	[X/H]	N
Li I	1.05	<1.30	⋯	⋯	6708
CH	8.43	7.43	0.17	−1.00	⋯
C$_2$	8.43	8.04	0.08	−0.39	⋯
CN	7.83	6.75	0.08	−1.08	⋯
O I	8.69	7.23	0.14	−1.46	3
Na I	6.24	3.68	0.13	−2.56	2
Mg I	7.60	3.77	0.08	−3.83	6
Al I	6.45	<1.50	⋯	<−4.95	3961
Si I	7.51	<3.30	⋯	<−4.21	3905
Ca II	6.34	1.60	0.18	−4.74	2
Ti II	4.95	<0.70	⋯	<−4.25	3760
Cr I	5.64	<1.50	⋯	<−4.14	4254
Fe I	7.50	2.01	0.14	−5.49	3
Ni I	6.22	<1.90	⋯	<−4.32	3858
Sr II	2.87	<−1.60	⋯	<−4.47	4077
Ba II	2.18	<−1.40	⋯	<−3.58	4554

Note. (1) Solar abundances from Asplund et al. (2009) $A_\odot(X) = \log \epsilon_\odot(X) = \log[N_\odot(X)/N_\odot(H)] + 12$ [X/H] $= A(X) - A_\odot(X) = \log \epsilon(X) - \log \epsilon_\odot(X)$. (2) Total abundance errors from the uncertainties in $\delta T_{\rm eff} = 100$ K, $\delta \log g = 0.20$ dex, $\delta \xi = 0.5$ km s^{-1}, and the statistical error. (3) Number of spectral features or wavelength in angstroms if only one feature.

spectrum (see Figure 1) using an automated fitting tool based on the IDL MPFIT[10] routine, with continuum location, global shift, abundance, and global FHWM as free parameters. We fit the CH lines of the G band in the spectral range $\lambda\lambda 426$–432 nm to obtain an average global (instrumental plus macroturbulent) Gaussian broadening (with no rotation) of $v_{\rm BR} = 7.5 \pm 0.1$ km s^{-1} and a carbon abundance $A(C) = 7.43 \pm 0.17$ dex. In Table 1 we provide the final abundances together with the total abundance error as the square root of the sum of all individual uncertainties in quadrature from $\delta T_{\rm eff} = 100$ K, $\delta \log g = 0.20$ dex, $\delta \xi = 0.5$ km s^{-1}, and the statistical abundance error. This carbon abundance is consistent with that reported in Aguado et al. (2018b) of $A(C) \sim 7.7$ dex, obtained from GTC/OSIRIS medium-resolution spectroscopy, taking into account the different effective temperatures adopted in that work. We have also analyzed the C$_2$ feature at 516.5 nm (see Figure 2), which shows a significantly higher abundance, $A(C) = 8.04 \pm 0.08$ dex. These discrepant C abundances from CH and C$_2$ features have been seen before in other C-enhanced metal-poor stars as the iron-poor star HE 0107-5240 (Christlieb et al. 2004). For the rest of the elements we fixed $v_{\rm BR} = 7.5$ km s^{-1} and derived the abundances by fitting short wavelength ranges (see Figure 2).

Table 1 summarizes our chemical abundance analysis of the HIRES spectrum of J0815+4729. We detect and provide 1D-LTE abundances for CH, C$_2$, CN, O, Na, Mg, Ca, and Fe and upper limits for Li, Al, Si, Ti, Cr, Ni, Sr, and Ba.

4.1. Iron, Oxygen, and Nitrogen

The iron abundance of J0815+4729 was measured from the three strongest Fe features, Fe I 371.9 nm, Fe I 382.0 nm, and Fe I 385.9 nm (see Figure 2). The line at Fe I 371.9 nm is on the wing of a Balmer line that is taken into account in the synthetic spectra. The quality of the blue part of the spectrum is limited,

---

[10] Available at http://purl.com/net/mpfit.

with an S/N ~ 30 inferred from the residuals of the fit. We thus fit the three features simultaneously to obtain a best-fit Fe abundance at $A(Fe) = 2.01 \pm 0.14$ in 1D-LTE. This Fe abundance determination makes J0815+4729 the fifth most iron-poor star known.

The oxygen abundance was measured from the simultaneous fit to the three lines of the O I triplet at λ 777 nm (see Figure 2), providing $A(O) = 7.23 \pm 0.14$ dex. The residuals of the fit indicate an S/N ~ 120. We also show for comparison the UVES spectrum of HE 1327−2326 (Frebel et al. 2008), where there is no clear detection of O I despite the higher quality (S/N ~ 250) of the UVES spectrum. The oxygen abundance of J0815+4729 is only ~ -1.5 dex below that of the Sun, indicating significant oxygen enrichment.

The nitrogen abundance was measured from the CN band at λ 388.3 nm (see Figure 2). We fix the C abundance to its best-fit value from the G band, leaving as a free parameter only the N abundance. The amount of nitrogen, [N/H] $= -1.08$, in J0815+4729 is also very high and very similar to that of the star HE 1327−2326.

4.2. Other Elements

Calcium and sodium were measured from the resonance lines, Ca II K $\lambda 393.3$ nm and Ca II H λ 396.8 nm, and Na I λ 588.9–589.5 nm. Magnesium abundance was derived from six lines of the two triplets at Mg I λ 382.9–383.8 nm and Mg I λ 516.7–518.3 nm. The typical dispersion of individual line abundances for Ca and Mg is 0.1 and 0.05 dex for Na, whereas the statistical error from individual fits is 0.04 dex. For the rest of the elements, we were only able to obtain upper limits from the strongest lines typically present in the spectra of iron-poor dwarf stars. In Table 1 we provide the abundance upper limit estimates together with the wavelength of the line used for each element.

4.3. Lithium

We were unable to detect lithium in the HIRES spectrum of J0815+4729. We derived an upper limit of $A(Li) < 1.3$ dex (see Figure 2) from the lithium doublet Li I λ 670.8 nm. Our J0815+4729 spectrum with an S/N ~ 120 is compared with the spectrum of HE 1327−2326, which has a lithium abundance limit $A(Li) < 0.7$ dex (Frebel et al. 2008), in contrast to the unambiguous lithium detection and abundance measurement of $A(Li) = 2.0$ dex found in the unevolved star J0023+0307 at the lowest iron abundance ([Fe/H] < -6.1; Aguado et al. 2019).

5. Discussion and Conclusions

The detection of the oxygen triplet in the spectrum of J0815+4729 is the first such detection in an extremely iron-poor star, anticipating a significant oxygen enhancement in this star with an oxygen-to-iron ratio [O/Fe] $= 4.03 \pm 0.12$. The lowest metallicity for which the O I had been previously detected is at [Fe/H] ~ -3.8 for the metal-poor giants CS 22949–037 and CS 29498–043, with oxygen abundances $A(O) = 8.3$ dex (Israelian et al. 2004) and at [Fe/H] $= -3.9$ for the metal-poor dwarf SDSS J2209–0028 (Spite et al. 2013) with an oxygen abundance $A(O) = 7.0$ dex and [O/Fe] ~ 2.2.

In Figure 3 we display the 1D-LTE oxygen-to-iron ratio, [O/Fe], versus the metallicity, [Fe/H], of J0815+4729 compared with literature measurements of other stars. This figure includes
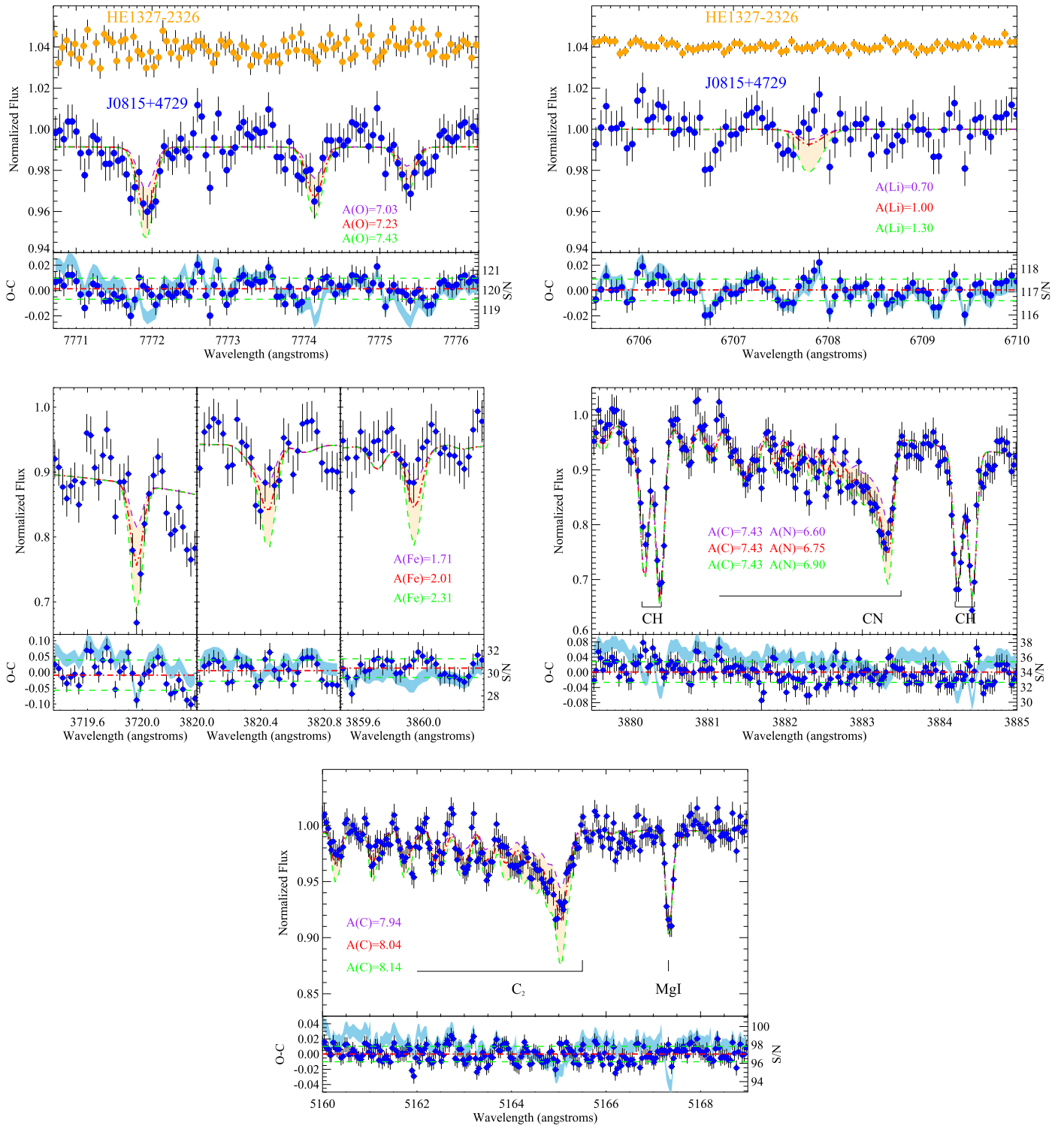
Figure 2. Specific spectral features in the Keck/HIRES spectrum of J0815+4729 (blue points with error bars), compared to SYNPLE synthetic spectra (the best-fit abundance is shown as red dashed–dotted lined). Shown are lines of oxygen (top left), lithium nondetection (top right), iron (middle left), nitrogen (middle right), and carbon C_2 (bottom). Top panels also show for comparison the UVES spectrum of HE 1327–2326 (Frebel et al. 2008), rebinned to the same wavelength step as the HIRES spectrum of J0815+4729. The bottom frame of each panel provides the residuals of the observations minus the best-fit model (blue points with error bars) and the uncertainty range (green dashed lines), and the signal-to-noise as the light blue curve.

only 1D-LTE oxygen measurements from different oxygen indicators, the [O I] forbidden line, the near-IR O I triplet, and the near-UV OH lines. A trend of increasing [O/Fe] toward lower metallicities is apparently seen. The [O/Fe] trend versus metallicity has been a matter of long discussions in the literature also related with the disagreement between different abundance indicators (see, e.g., González Hernández et al. 2010, and references therein). Recent results in 3D and NLTE seem to confirm an increasing trend [O/Fe] toward lower metallicities, in particular, at the lowest metallicities for all O abundance indicators (González Hernández et al. 2010; Amarsi et al. 2015). The upturn of [O/Fe] at the lowest metallicities ($-3.5 <$ [Fe/H] < -2.5)
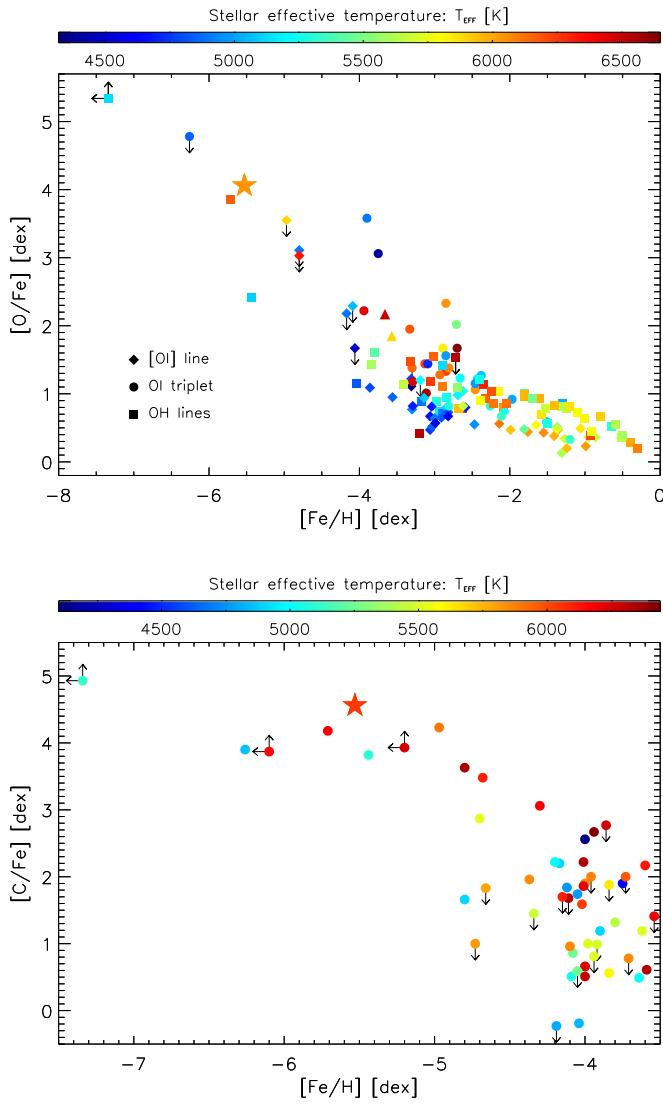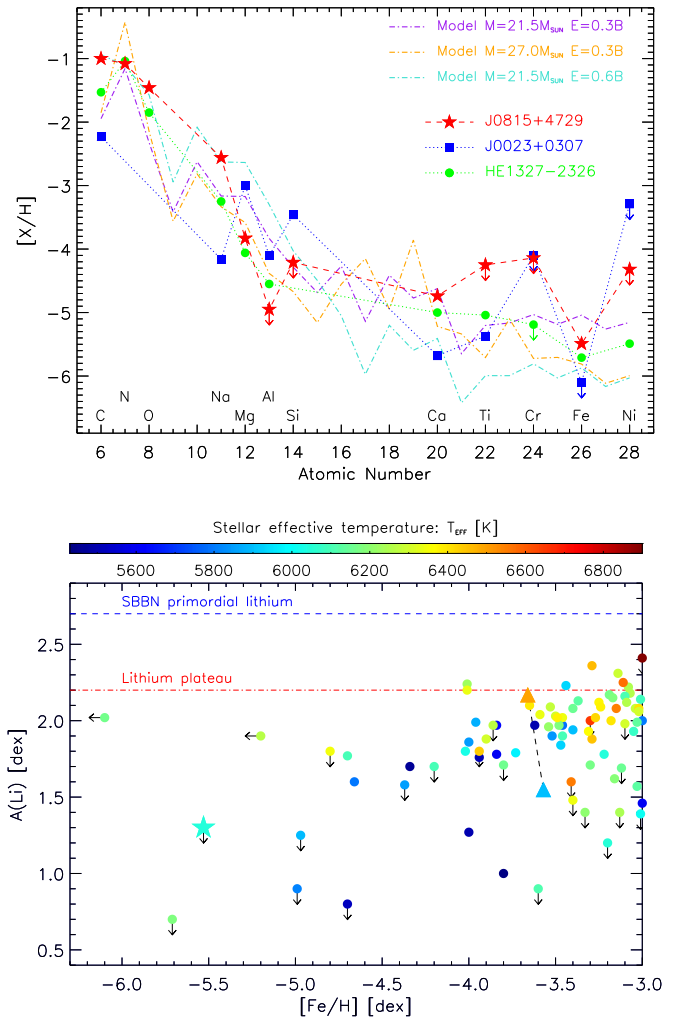
Figure 3. Top: 1D-LTE oxygen-to-iron abundance ratios [O/Fe] vs. metallicity [Fe/H] of J0815+4729 (large star symbol) compared with literature measurements from the [O I] forbidden line (diamonds), the near-IR O I triplet (circles), and the near-UV OH lines (squares). The two triangles at [Fe/H] ∼ −3.6 correspond to the oxygen measurement from OH lines in the metal-poor binary stars CS 22876–032 AB (González Hernández et al. 2008). Bottom: 1D-LTE carbon abundance vs. [Fe/H] of J0815+4729 (large star symbol) compared with literature measurements for stars with [Fe/H] < −3.5 (small circles). In both panels, symbols are colored by their corresponding effective temperature. Upward and left-pointing arrows indicate lower and upper limits.

Figure 4. Top: 1D-LTE abundance pattern of J0815+4729 (red stars) compared to the abundance pattern of two iron-poor stars with similar effective temperature and iron content: J0023+0307 (Aguado et al. 2019, blue squares) and HE 1327–2326 (Frebel et al. 2008, green circles). Upper limits are indicated by downward arrows. Bottom: lithium abundance vs. [Fe/H] for J0815+4729 compared with literature measurements for unevolved stars with [Fe/H] < −3.0 and log g > 3.0. In both panels, symbols are colored by their corresponding effective temperature. The two large triangles connected with a black dashed line correspond to the metal-poor binary CS 22876–032 AB (González Hernández et al. 2008, 2019). Downward and left-pointing arrows indicate upper limits. The blue dashed line is the predicted SBBN primordial lithium abundance, and the red dashed–dotted line is the value of the lithium plateau, known as the Spite Plateau.

may indicate a shift toward more massive SNe, more metal-poor SNe, and hypernovae at earlier epochs, thus is expected to yield larger [O/Fe] ratios (Kobayashi et al. 2006).

The two giant stars CS 22949–037 and CS 29498–043 also show high Mg and Si abundances, and lower Na and Al abundances, displaying an "odd–even" pattern also seen in the metal-poor stars J2217+2104 (Aoki et al. 2018) and J0023 +0307 (Aguado et al. 2019). This odd–even pattern has been associated with massive pair-stability SNe (PISNe; e.g., Heger & Woosley 2002). Figure 4 compares the abundance pattern of J0815+4729 to those of the two iron-poor stars HE 1327–2326 and J0023+0307, which have similar stellar parameters and iron content. PISNe models predict element abundance ratios [Na/Mg] = −1.5 and [Ca/Mg] ∼ 0.5–1.3 (Takahashi et al. 2018). While each one of these ratios, [Na/Mg] = −1.16 in

J0023+0307 and [Ca/Mg] = 0.94 in HE 1327–2326, are marginally consistent with PISNe predictions, the observed abundance ratios of J0815+4729, [Na/Mg] = 1.27 and [Ca/Mg] = −0.91 rule out any contamination from PISNe.

J0815+4729 shows a particularly large enhancement of CNO elements with 1D-LTE ratios [X/Fe] of 4.49, 4.41, and 4.03 for C, N, and O, respectively. J0815+4729 shows significantly higher C abundance than HE 1327–2326 and J0023+0307 (see Figures 3 and 4). The amount of N is slightly lower than C in J0815+4729, while HE 1327–2326 shows significantly higher N to C abundance by 0.5 dex. Oxygen, however, is lower than C by 0.5 and 0.3 dex in J0815+4729 and HE 1327–2326, respectively. There is so far no evidence for RV variations nor any chemical signature of mass transfer from (prior) companion AGB stars to any of these three metal-poor unevolved stars. Their location in the A(C) versus [Fe/H]

diagram is coincident with CEMP-no (Bonifacio et al. 2015) stars, which are predicted to be the direct descendants of the first generation of stars, with atmospheric abundances (including vast amounts of carbon) reflecting nucleosynthesis yields from one or a few zero-metallicity core-collapse SNe diluted with the primordial gas. J0815+4729 appears to be consistent with the upper envelope of the low-carbon band in the A(C)–[Fe/H] diagram (Spite et al. 2013; Yoon et al. 2016). The extremely high CNO abundances, coupled with high Na and Mg abundances (see Figure 4), suggests a fallback model in which some of the Ca and Fe fall back into the black hole (Umeda & Nomoto 2003). The low [Mg/C] = −2.83 and high [Mg/Fe] = 1.66 and [Ca/Fe] = 0.75 ratios in J0815+4729 can also be explained by a mono-enriched scenario (i.e., one SN per mini-halo) based on the divergence model of the chemical displacement from Hartwig et al. (2018). On the other hand, the [Al/Mg] < −1.12 and [N/Na] = 1.48 abundance ratios suggest a multi-enriched scenario. In either case, the similarity between the abundance patterns of J0815+4729 and HE 1327–2326 points to enrichment from a Population III SN progenitor with mass between 15 $M_\odot$ (Ishigaki et al. 2018) and 27 $M_\odot$ (Heger & Woosley 2010). We have used the STARFIT[11] code (Heger & Woosley 2010) to fit the observed abundances. In Figure 4 we show several metal-free SN models with masses 21.5–27 $M_\odot$ and energies 0.3–0.6B (1 B = 1 Bethe = 10^{51} erg). All three of these low-energy SN models with very little mixing seem to fit reasonably well the observed abundances.

Metal-poor damped Lyman α (DLA) systems show abundance ratios [C/O] $\sim$ −0.3, well explained with core-collapse Population III SN models (with low kinetic energies at 1×10^{51} erg) and a typical progenitor mass of 20 $M_\odot$ (Cooke et al. 2017). Similarly, halo metal-poor dwarf stars (e.g., Amarsi et al. 2019) have [C/O] $\sim$ −0.5, consistent with DLAs. The 1D-LTE [C/O] abundance ratio of J0815+4729 is $\sim$0.5, and thus is significantly higher than both ratios, but this value may be affected by 3D-NLTE effects that would possibly lower this ratio (Behara et al. 2010; Amarsi et al. 2019).

The absence of detectable lithium in the spectrum of J0815 +4729 at a limit of A(Li) < 1.3 dex exacerbates the cosmological lithium depletion problem. Figure 4 displays the Li abundances of unevolved Galactic stars with [Fe/H] < −3. Most of these stars have A(Li) $\sim$ 2.0 dex, with a different degree of Li depletion at increasingly higher temperature and decreasing metallicity (Bonifacio et al. 2018; González Hernández et al. 2019). There is a clear lack of stars between this upper envelope defined by the lithium plateau (A(Li) $\sim$ 2.2; Spite & Spite 1982; Rebolo et al. 1988) and the primordial Li abundance predicted by the standard Big Bang nucleosynthesis (SBBN; A(Li) $\sim$ 2.7; Cyburt et al. 2016).

At [Fe/H] < −3.5, only three stars show Li measurements at A(Li) = 2.2 (González Hernández et al. 2008, 2019; Bonifacio et al. 2018). Matsuno et al. (2017) have suggested that most stars at [Fe/H] < −4.5 show Li abundances or upper limits A(Li) < 1.8 dex, and conclude that there is no clear connection between the amount of carbon and the Li content. Among the four unevolved stars with [Fe/H] < −5, all C-enhanced, only two stars have Li detections with abundances close to the Li plateau: J0023+0307 with A(Li) $\sim$ 2.0 dex (Aguado et al. 2019) and J0135+0641 with A(Li) $\sim$ 1.9 dex (Bonifacio et al. 2018). HE 1327–2326 and J0815+4729 with the strongest

carbon enhancement among stars with [Fe/H] < −5 do not show any Li detection. Any model claiming a solution to the cosmological lithium problem must explain the more than 1 dex Li abundance variance among these stars.

ORCID iDs

Jonay I. González Hernández https://orcid.org/0000-0002-0264-7356
David S. Aguado https://orcid.org/0000-0001-5200-3973
Carlos Allende Prieto https://orcid.org/0000-0002-0084-572X
Adam J. Burgasser https://orcid.org/0000-0002-6523-9536
Rafael Rebolo https://orcid.org/0000-0003-3767-7085

References

Aguado, D. S., Allende Prieto, C., González Hernández, J. I., & Rebolo, R. 2018a, ApJL, 854, L34
Aguado, D. S., González Hernández, J. I., Allende Prieto, C., & Rebolo, R. 2017, A&A, 605, A40
Aguado, D. S., González Hernández, J. I., Allende Prieto, C., & Rebolo, R. 2018b, ApJL, 852, L20
Aguado, D. S., González Hernández, J. I., Allende Prieto, C., & Rebolo, R. 2019, ApJL, 874, L21
Amarsi, A. M., Asplund, M., Collet, R., & Leenaarts, J. 2015, MNRAS, 454, L11
Amarsi, A. M., Nissen, P. E., Asplund, M., Lind, K., & Barklem, P. S. 2019, A&A, 622, L4
Aoki, W., Matsuno, T., Honda, S., et al. 2018, PASJ, 70, 94
Asplund, M., Grevesse, N., Sauval, A. J., & Scott, P. 2009, ARA&A, 47, 481
Barklem, P. S., Christlieb, N., Beers, T. C., et al. 2005, A&A, 439, 129
Behara, N. T., Bonifacio, P., Ludwig, H.-G., et al. 2010, A&A, 513, A72
Bonifacio, P., Caffau, E., Spite, M., et al. 2015, A&A, 579, A28
Bonifacio, P., Caffau, E., Spite, M., et al. 2018, A&A, 612, A65
Caffau, E., Bonifacio, P., François, P., et al. 2012, A&A, 542, A51
Casagrande, L., Ramírez, I., Meléndez, J., Bessell, M., & Asplund, M. 2010, A&A, 512, A54
Christlieb, N., Green, P. J., Wisotzki, L., & Reimers, D. 2001, A&A, 375, 366
Christlieb, N., Gustafsson, B., Korn, A. J., et al. 2004, ApJ, 603, 708
Cooke, R. J., Pettini, M., & Steidel, C. C. 2017, MNRAS, 467, 802
Cyburt, R. H., Fields, B. D., Olive, K. A., & Yeh, T.-H. 2016, RvMP, 88, 015004
Dawson, K. S., Schlegel, D. J., Ahn, C. P., et al. 2013, AJ, 145, 10
Frebel, A., Collet, R., Eriksson, K., Christlieb, N., & Aoki, W. 2008, ApJ, 684, 588
González Hernández, J. I., & Bonifacio, P. 2009, A&A, 497, 497
González Hernández, J. I., Bonifacio, P., Caffau, E., et al. 2019, A&A, 628, A111
González Hernández, J. I., Bonifacio, P., Ludwig, H.-G., et al. 2008, A&A, 480, 233
González Hernández, J. I., Bonifacio, P., Ludwig, H.-G., et al. 2010, A&A, 519, A46
Hansen, T., Hansen, C. J., Christlieb, N., et al. 2014, ApJ, 787, 162
Hartwig, T., Yoshida, N., Magg, M., et al. 2018, MNRAS, 478, 1795
Heger, A., & Woosley, S. E. 2002, ApJ, 567, 532
Heger, A., & Woosley, S. E. 2010, ApJ, 724, 341
Ishigaki, M. N., Tominaga, N., Kobayashi, C., & Nomoto, K. 2018, ApJ, 857, 46

---

[11] http://starfit.org

Israelian, G., Shchukina, N., Rebolo, R., et al. 2004, A&A, 419, 1095
Keller, S. C., Bessell, M. S., Frebel, A., et al. 2014, Natur, 506, 463
Keller, S. C., Schmidt, B. P., Bessell, M. S., et al. 2007, PASA, 24, 1
Kobayashi, C., Umeda, H., Nomoto, K., Tominaga, N., & Ohkubo, T. 2006, ApJ, 653, 1145
Koesterke, L., Allende Prieto, C., & Lambert, D. L. 2008, ApJ, 680, 764
Li, H., Tan, K., & Zhao, G. 2018, ApJS, 238, 16
Matsuno, T., Aoki, W., Suda, T., & Li, H. 2017, PASJ, 69, 24
Mészáros, S., Allende Prieto, C., Edvardsson, B., et al. 2012, AJ, 144, 120
Nordlander, T., Bessell, M. S., Da Costa, G. S., et al. 2019, MNRAS, 488, L109
Rebolo, R., Beckman, J. E., & Molaro, P. 1988, A&A, 192, 192

Schlegel, D. J., Finkbeiner, D. P., & Davis, M. 1998, ApJ, 500, 525
Sestito, F., Longeard, N., Martin, N. F., et al. 2019, MNRAS, 484, 2166
Spite, M., Caffau, E., Bonifacio, P., et al. 2013, A&A, 552, A107
Spite, M., & Spite, F. 1982, Natur, 297, 483
Starkenburg, E., Aguado, D. S., Bonifacio, P., et al. 2018, MNRAS, 481, 3838
Starkenburg, E., Martin, N., Youakim, K., et al. 2017, MNRAS, 471, 2587
Takahashi, K., Yoshida, T., & Umeda, H. 2018, ApJ, 857, 111
Umeda, H., & Nomoto, K. 2003, Natur, 422, 871
Vogt, S. S., Allen, S. L., Bigelow, B. C., et al. 1994, Proc. SPIE, 2198, 362
Yoon, J., Beers, T. C., Placco, V. M., et al. 2016, ApJ, 833, 20
York, D. G., Adelman, J., Anderson, J. E., Jr., et al. 2000, AJ, 120, 1579